Inorg. Chem. **2006**, *45*, 3048–3056

Structure and Photochemical Properties of (μ-Alkoxo)bis(μ-carboxylato)diruthenium Complexes with Naphthylacetate Ligands

Misaki Nakai,[†] Takuzo Funabiki,[‡] Chikara Ohtsuki,[§] Masafumi Harada,[||] Akio Ichimura,[⊥] Rika Tanaka,[⊥] Isamu Kinoshita,[⊥] Masahiro Mikuriya,[#] Hiroaki Benten,[£] Hideo Ohkita,[£] Shinzaburo Ito,[£] Makoto Obata,[†] and Shigenobu Yano*[,†]

Division of Material Science, Graduate School of Humanities and Sciences, Nara Women's University, Kitauoyanishimachi, Nara 630-8506, Japan, Biomimetic Research Center, Doshisha University, Kyo-Tanabe 610-0321, Japan, Graduate School of Materials Science, Nara Institute of Science and Technology, 8916-5 Takayamacho, Ikoma 630-0101, Japan, Faculty of Human Life and Environment, Nara Women's University, Kitauoyanishimachi, Nara 630-8506, Japan, Graduate School of Molecular Material Science, Osaka City University, Sumiyoshiku, Osaka 577-8502, Japan, School of Science and Technology, Kwansei Gakuin University, 2-1 Gakuen, Sanda 669-1337, Japan, and Department of Polymer Chemistry, Graduate School of Engineering, Kyoto University, Kyoto Daigaku Katsura, Nishikyo-ku, Kyoto 615-8510, Japan

Received September 15, 2005

Two new dinuclear Ru(III) complexes containing naphthalene moieties, $K[Ru_2(dhpta)(\mu\text{-}O_2CCH_2\text{-}1\text{-}naph)_2]$ (**1**) and $K[Ru_2(dhpta)(\mu\text{-}O_2CCH_2\text{-}2\text{-}naph)_2]$ (**2**) (H_5dhpta = 1,3-diamino-2-hydroxypropane-*N,N,N′,N′*-tetraacetic acid, naph-1-CH_2CO_2H = 1-naphthylacetic acid, naph-2-CH_2CO_2H = 2-naphthylacetic acid), were synthesized. Complex **2** crystallized as an orthorhombic system having a space group of *Pbca* with unit cell parameters $a = 10.6200(5)$ Å, $b = 20.270(1)$ Å, $c = 35.530(2)$ Å, and $Z = 8$. EXAFS analysis of **1** and **2** in the solid states and in solution clarified that the dinuclear structures of **1** and **2** were kept in DMSO solutions. Variable-temperature magnetic susceptibility data indicated that the two Ru(III) centers are strongly antiferromagnetically coupled as shown by the large coupling constants, $J = -581$ cm^{-1} (**1**) and -378 cm^{-1} (**2**). In the cyclic voltammograms of **1** and **2**, one oxidation peak and two reduction peaks which were assigned to the redox reaction of the ruthenium moieties were observed in DMF. The large conproportionation constants estimated from the reduction potentials of $Ru^{III}Ru^{III}$ and $Ru^{III}Ru^{II}$ indicated the great stability of the mixed-valent state. The mixed-valent species $[Ru^{III}Ru^{II}(dhpta)(\mu\text{-}O_2CCH_2\text{–}R)_2]^{2-}$ (R = 1-naph (**6**) and R = 2-naph (**7**)) were prepared by controlled potential electrolysis of **1** and **2** in DMF. The electronic absorption spectra of **6** and **7** were similar to that of $[Ru^{III}Ru^{II}(dhpta)(\mu\text{-}O_2CCH_3)_2]^{2-}$ which is a typical Class II type mixed-valent complex. The fluorescence decay of **1** and **2** indicated that there are two quenching processes which come from the excimer and monomer states. The short excimer lifetimes of **1** and **2** were ascribed to the energy transfer from the naphthyl moieties to the Ru centers. The different excimer ratio between **1** and **2** suggested that the excimer formation is affected by the conformation of the naphthyl moieties in the diruthenium(III) complexes.

Introduction

Molecular- and supramolecular-based systems have attracted much attention because the construction and development of these systems may enable the absorption of sunlight and the conversion of the solar energy to useful and storable artificial energy forms. To convert solar energy to chemical

* To whom correspondence should be addressed. Phone and Fax: +81-742-20-3392. E-mail: yano@cc.nara-wu.ac.jp.
[†] Graduate School of Humanities and Sciences, Nara Women's University.
[‡] Biomimetic Research Center, Doshisha University.
[§] Graduate School of Materials Science, Nara Institute of Science and Technology.
[||] Faculty of Human Life and Environment, Nara Women's University.
[⊥] Graduate School of Molecular Material Science, Osaka City University.
[#] School of Science and Technology, Kwansei Gakuin University.
[£] Graduate School of Engineering, Kyoto University.

10.1021/ic051582u CCC: $33.50 © 2006 American Chemical Society
Published on Web 03/04/2006

energy in these systems, it is important to construct efficient photoinduced electron- and energy-transfer processes. Since photoinduced electron-transfer involves an electron-transfer process from an electron-donating species to an electron-accepting species,[1,2] many efforts have been made for the synthesis and characterization of electron-donors (e. g., porphyrin derivatives,[3] naphthalene,[4] and pyrene[5]) and electron-acceptors (e. g., quinoline,[6] fullerene,[7−10] and metal complexes[11−15]).

Recently, many proteins involving multiiron centers, such as ferredoxin,[16] hemerythrin,[16−19] ribonucleotide reductases,[16,17,20] and methane monooxygenases,[17,21−29] have been shown to play key roles for the elaborate electron transfer in the biological systems. Since the diiron complexes have the ability of electron donors to act as an electron pool, it is well expected that the introduction of photofunctional moieties to model diiron complexes for these diiron proteins will lead to the development of new artificial solar energy harvesting systems. Considering the presumed high barriers in controlling the electronic states of diiron centers, we have chosen diruthenium complexes ligated by photofunctional moieties as probable new systems. Ruthenium, which is not involved in the active sites of metalloproteins, belongs to the same group as iron, and the diruthenium centers have the potential to provide redox chemistry in a manner similar to that of diiron. Compared with diiron complexes, diruthenium complexes are expected to exhibit stabilized mixed-valent states, which are advantageous for the catalytic redox reaction. Some examples of mixed-valent ruthenium complexes have been reported (e.g., $[(NC)_5Ru^{II}CNRu^{III}(NH_3)_5]^-$,[30] $[(NH_3)_5Ru^{II}LRu^{III}L']^+$ (L = pyrazine, L′ = EDTA),[31] and $[(bpy)_2Ru^{III}$(L-SP-L)$Ru^{II}(decbpy)_2]^{5+}$ (bpy = 2,2′-bipyridine, decbpy = 4,4′-diethoxycarbonyl-2,2′-bipyridine, L = 2-(2′-pyridyl)benzimidazolyl, SP = $-(CH_2)_n-$),[32] which were studied on the basis of their photochemical properties and electron or energy transfer. Furthermore, dinuclear complexes, $Rh^{III}(dcb)_2$-(BL)-$Ru^{II}(dmp)_2$ and $Rh^{III}(dcb)_2$-(BL)-Ru^{II}-$(bpy)_2$ (dcb = 4,4′-dicarboxy-2,2′-bipyridine, dmp = 4,7-dimethyl-1,10-phenanthroline, BL = 1,2-bis[4-(4′-methyl-2,2′-bipyridyl)]ethane), have been shown to exhibit faster (10^8-10^9 s^{-1}) and more efficient (>95%) photoinduced electron transfer than the mononuclear complex, $Ru^{II}(dcb)_2$-(dmb) (dmb = 4,4′-dimethyl-2,2′-bipyridine).[33]

Recently, we synthesized and characterized $K[Ru_2(dhpta)(\mu\text{-}O_2CCH_3)_2]$ (**3**) (H_5dhpta = 1,3-diamino-2-hydroxypropane-*N*,*N*,*N*′,*N*′-tetraacetic acid).[34] We have found that $K[Ru_2(dhpta)(\mu\text{-}O_2CC_6H_5)_2]$ (**4**) can be synthesized by replacing the acetate moieties of **3** with benzoate.[35] Using this ligand substitution reaction, we synthesized $K[Ru_2(dhpta)(\mu\text{-}O_2C\text{-}p\text{-}ZnTPP)_2]$ (**5**) (ZnTPP-*p*-CO_2H = zinc 5-(4-carboxylphenyl)-10,15,20-triphenylporphyrin)[36] to introduce two bridging porphyrin moieties into the diruthenium complex, in which two porphyrin moieties are expected to be effective for photoinduced charge separation as porphyrin dimers. In the photosynthesis, two bacteriochlorophylls play key roles as the special pair for light absorption, charge separation, and electron transfer to two bacteriopheophytins and two quinolines.[16] By mimicking this special pair, many dimers of porphyrins and derivatives thereof have been studied so far.[37,38] Kobuke et al. synthesized a cofacial dimer

(1) Piotrowiak, P.; Rodgers, M. A. J. In *Electron Transfer in Chemistry V*; Balzani, V., Ed.; Vch Verlagsgesellschaft Mbh: Weinheim, Germany, 2001; Vol. I−V.
(2) Connolly, J. S.; Bolton, J. R.; Fox, M. A. In *Photoinduced Electron Transfer*; Chanon, M., Ed.; Elsevier Science: Oxford, 1988.
(3) Aspley, C. J.; Smith, J. R. L.; Perutz, R. N. *J. Chem. Soc., Dalton Trans.* **1999**, *14*, 2269.
(4) Kobayashi, N.; Lam, H.; Nevin, W. A.; Janda, P.; Leznoff, C. C. *Inorg. Chem.* **1990**, *29*, 3415.
(5) Harriman, A.; Hissler, M.; Khatyr, A.; Ziessel, R. *Chem. Commun.* **1999**, 735.
(6) Gust, D.; Moore, T. A. *Science* **1989**, *244*, 35.
(7) Luo, C.; Guldi, D. M.; Imahori, H.; Tamaki, K.; Sakata, Y. *J. Am. Chem. Soc.* **2000**, 122, 6535.
(8) Liddel, P. A.; Kuciauskas, D.; Sumida, J. P.; Nash, B.; Nguyen, D.; Moore, A. L.; Moore, T. A.; Gust, D. *J. Am. Chem. Soc.* **1997**, *119*, 140.
(9) Imahori, H.; Tamaki, K.; Guldi, D. M.; Luo, C.; Ito, O.; Sakata, Y.; Fukuzumi, S. *J. Am. Chem. Soc.* **2001**, *123*, 2607.
(10) El-Khouly, M. E.; Ito, O.; Smith, P. M.; D'Souza, F. J. *J. Photochem. Photobiol. C.* **2004**, *5*, 79.
(11) Rowley, N. M.; Kurek, S. S.; George, M. W.; Hubig, S. M.; Beer, P. D.; Jones, C. J.; Kelly, J. M.; McCleverty, J. A. Y. *J. Chem. Soc., Chem. Commun.* **1992**, 497.
(12) Wall, M. H. J.; Akimoto, S.; Yamazaki, T.; Ohta, N.; Yamazaki, I.; Sakuma, T.; Kido, H. *Bull. Chem. Soc. Jpn.* **1999**, *72*, 1475.
(13) Rowley, N. M.; Kurek, S. S.; Foulon, J.-D.; Hamor, T. A.; Jones, C. J.; McCleverty, J. M.; Hubig, S. M.; McInnes, E. J. L.; Payne, N. N.; Yellowlees, L. J. *Inorg. Chem.* **1995**, *34*, 4414.
(14) Rowley, N. M.; Kurek, S. S.; Ashton, P. R.; Hamor, T. A.; Jones, C. J.; Spencer, N.; McCleverty, J. A.; Beddard, G. S.; Feehan, T. M.; White, N. T. H.; McInnes, E. J. L.; Payne, N. N.; Yellowlees, L. J. *Inorg. Chem.* **1996**, *35*, 7526.
(15) Londergan, C. H.; Salsman, J. C.; Ronco, S.; Dolkas, L. M.; Kubiak, C. P. *J. Am. Chem. Soc.* **2002**, *124*, 6236.
(16) Lippard, S. J.; Berg, J. M. *Principles of Bioinorganic Chemistry*; University Science Books: Mill Valley, CA, 1994.
(17) Tshuva, E. Y.; Lippard, S. J. *Chem. Rev.* **2004**, *104*, 987.
(18) Friesner, R. A.; Baik, M.; Gherman, B. F.; Guallar, V.; Wiestam, M.; Murphy, G. R. B.; Lippard, S. J. *Coord. Chem. Rev.* **2003**, *267*, 238.
(19) Stenkamp, R. E.; Sieker, L. C.; Jensen, L. H.; McCallum, J. D.; Sandersloehr, J. *Proc. Natl. Acad. Sci.* **1985**, *82*, 1104.
(20) Jordan, A.; Reichard, P. *Annu. Rev. Biochem.* **1998**, *67*, 67.
(21) Merkx, M.; Kopp, D. A.; Sazinsky, M. H.; Blazyk, J. L.; Müller, J.; Lippard, S. J. *Angew. Chem., Int. Ed.* **2001**, *40*, 4000.
(22) Westerheide, L.; Pascaly, M.; Krebs, B. *Curr. Opin. Chem.* **2000**, *4*, 235.
(23) Rosenzweig, A. C.; Feng, X.; Lippard, S. J. In *Applications of Enzyme Biotechnology*; Kelly. J. W., Baldwin, T. O., Eds.; Plenum Press: New York, 1991.
(24) Whittington, D. A.; Lippard, S. J. *J. Am. Chem. Soc.* **2001**, *123*, 827.
(25) Rosenzweig, A. C.; Nordlind, P.; Takahara, P. M.; Frederick, C. A.; Lippard, S. J. *Chem. Biol.* **1995**, *2*, 409.
(26) Rosenzweig, A. C.; Frederick, C. A.; Lippard, S. J.; Nordlund, P. *Nature* **1993**, *366*, 537.
(27) Shu, L. J.; Nesheim, J. C.; Kauffmann, K.; Münck, E.; Lipscomb, J. D.; Que, L., Jr. *Science* **1997**, *275*, 515.
(28) Valentine, A. M.; Stahl, S. S.; Lippard, S. J. *J. Am. Chem. Soc.* **1999**, *121*, 3876.
(29) Lipscomb, J. D.; Que, L., Jr. *J. Biol. Inorg. Chem.* **1998**, *3*, 331.
(30) Doorn, S. K.; Stoutland, P. O.; Dyer, R. B.; Woodruff, W. H. *J. Am. Chem. Soc.* **1992**, *114*, 3133.
(31) Creutz, C.; Kroger, P.; Matsubara, T.; Netzel, T. L.; Sutin, N. *J. Am. Chem. Soc.* **1979**, *101*, 5442.
(32) Nozaki, K.; Ohno, T. *Coord. Chem. Rev.* **1994**, *132*, 215.
(33) Kleverlaan, C. J.; Indelli, M. T.; Bignozzi, C. A.; Pavanin, L.; Scandola, F.; Hasselman, G. M.; Meyer, G. J. *J. Am. Chem. Soc.* **2000**, *122*, 2840.
(34) Tanase, T.; Yamada, Y.; Tanaka, K.; Miyazu, T.; Kato, M.; Lee, K.; Sugihara, Y.; Mori, W.; Ichimura, A.; Kinoshita, I.; Yamamoto, Y.; Haga, M.; Sasaki, Y.; Yano, S. *Inorg. Chem.* **1996**, *35*, 6230.
(35) Takagi, H.; Ichimura, A.; Yano, S.; Kinoshita, I.; Isobe, K.; Abe, M.; Sasaki, Y.; Mikata, Y.; Tanase, T.; Takeshita, N.; Inoue, C.; Kimura, Y.; Endo, S.; Tamura, K.; Yano, S. *Electrochemistry* **1999**, *67*, 1192.
(36) Tanihara, N.; Obata, M.; Harada, M.; Mikata, Y.; Hamazawa, A.; Kinoshita, I.; Isobe, K.; Ichimura, A.; Hoshino, M.; Mikuriya, M.; Yano, S. *Inorg. Chem. Commun.* **2003**, *6*, 447.

of imidazolyl-substituted zinc porphyrin.[39] Compared with the monomeric porphyrin, the dimer formation accelerated the charge separation rate and decelerated the charge recombination rate, resulting in the prolonged charge separation state of porphyrin. For complex **5**, however, no elongation of the charge separation state by the interaction between the two porphyrins was found, while an electron transfer between ruthenium centers and porphyrin moieties was observed.[40]

Since the discovery of the excimer emission of pyrene by Förster and Kasper in 1954,[41] excimer fluorescences have been observed for a large number of aromatic hydrocarbons.[42] Naphthalene and its derivatives are sometimes used as fluorescence probes[43] and metal ion sensors[44,45] by taking advantage of the excimer emission. With this connection, the excimer-mediated photoinduced energy transfer, which plays an important role in wide areas of photochemistry and photobiology including light harvesting and energy storage processes,[46,47] has been extensively studied. However, the essential conformational dynamics in the field of intramolecular excimer formation are not clear yet. The relationship between a metal cluster and a naphthyl excimer has been studied by Picraux et al.,[48] who synthesized a diiron complex, $[Fe_2(O)(\mu\text{-}O_2CCH_2\text{-}2\text{-}naph)_2(TACN\text{-}Me_3)_2]^{2+}$ (TACN-Me_3 = 1,4,7-trimethyl-1,4,7-triazacyclonane), and reported that the energy transfer occurs from the naphthyl moieties to the iron centers via an excimer state. This important result encouraged us to examine the possibility of photoinduced energy transfer between a ruthenium cluster and naphthyl moieties in the diruthenium complexes, $K[Ru_2(dhpta)(\mu\text{-}O_2CCH_2\text{-}1\text{-}naph)_2]$ (**1**) and $K[Ru_2(dhpta)(\mu\text{-}O_2CCH_2\text{-}2\text{-}naph)_2]$ (**2**).

Experimental Section

General Procedures. All reagents were commercial products and were used without further purification. $RuCl_2(DMSO)_4$[49] and $K[Ru_2(dhpta)(\mu\text{-}O_2CCH_3)_2]$ (**3**)[34] were prepared according to the previous paper.

$K[Ru_2(dhpta)(\mu\text{-}O_2CCH_2\text{-}1\text{-}naph)_2]$ (1). $RuCl_2(DMSO)_4$ (1.008 g, 2.080 mmol) was added to an aqueous solution (pH 5) of H_5-dhpta (0.345 g, 1.071 mmol), and the mixture was heated at 80 °C. While the pH was maintained at 5 by the addition of aqueous KOH, the reaction mixture was stirred for 6 h at 80 °C. A MeOH−water solution (30 mL, v/v = 1/1) of 1-naphthylacetic acid (0.446 g, 2.395 mmol) was added to the mixture, and it was stirred at 80 °C for 2 days. A MeOH−water solution (30 mL, v/v = 1/1) of 1-naphthylacetic acid (0.419 g, 2.250 mmol) was added to the mixture, and it was stirred for 5 h at 80 °C. The dark red solution was concentrated in vacuo, and the precipitates were filtered off. The precipitates were dissolved in MeOH and purified by gel permeation chromatography (Sephadex LH-20 ϕ = 3 cm, h= 70 cm, eluted by MeOH). The dark red band was collected and concentrated to yield a dark red powder. Yield: 178 mg (9.2%). Anal. Calcd for $C_{35}H_{33}KN_2O_{14}Ru_2$ ($K[Ru_2(dhpta)(\mu\text{-}O_2CCH_2\text{-}1\text{-}naph)_2]\cdot H_2O$): C, 44.39; H, 3.51; N, 2.96; Found: C, 44.30; H, 3.64; N, 2.98. ESI MS: *m*/*z* 891.2 $[M - K]^-$ (calcd for $C_{35}H_{31}N_2O_{13}Ru_2$, 891.0) UV−vis ($c$ = 0.242 mM, dimethyl sulfoxide (DMSO), light path length = 1 cm): λ, nm (ϵ, $M^{-1}\,cm^{-1}$) 285 (2.06×10^4), 381 (2.37×10^3), 491 (2.66×10^3). ^{1}H NMR in DMSO-d_6 (300.07 MHz): δ 61.9 (br, 1H, 2-dhpta*H*), 9.00 (br, 1H, H9′-naphthyl), 7.78−7.70 (3H, m, H6, H7, H9-naphthyl), 7.53 (d, 1H, ^3J = 8.1 Hz, H4-naphthyl), 7.38−7.11 (m, 6H, H2, H3, H3′, H4′, H8, H8′-naphthyl), 6.77 (dd, 1H, ^3J = 7.2 and 8.1 Hz, H7′-naphthyl), 5.49 (s, 2H, $-CH_2'$-naphthyl), 5.06 (d, 1H, ^3J = 8.1 Hz, H2′-naphthyl), 4.32 (d, 1H, H6-naphthyl), 3.95 (br, 2H, 1,3-dhpta*H*), −0.99 (d, 2H, ^2J = 17.4 Hz, $-N-CH_2-CO_2$), −1.69 (s, 2H, $-CH_2$-naphthyl), −2.84 (d, 2H, ^2J = 18.0 Hz, $-N-CH_2-CO_2$), −6.04 (d, 2H, ^2J = 11.1 Hz, 1,3-dhpta*H*′), −6.69 (d, 2H, ^2J = 11.1 Hz, $N-CH_2'$-CO_2), −6.85 (d, 2H, ^2J = 16.2 Hz, $N-CH_2'$-CO_2). IR (KBr, cm^{-1}): 3425, 2361, 2341, 1663, 1564, 1508, 1391, 1348, 1308.

$K[Ru_2(dhpta)(\mu\text{-}O_2CCH_2\text{-}2\text{-}naph)_2]$ (2). 2-Naphthylacetic acid (806 mg, 4.328 mmol) was added to the MeOH solution (200 mL) of $K[Ru_2(dhpta)(\mu\text{-}O_2CCH_3)_2]$ (202 mg, 0.297 mmol), and the mixture was refluxed for 3 days. The mixture was concentrated in vacuo and purified by gel permeation chromatography (Sephadex LH-20 ϕ = 3 cm, h = 70 cm, eluted by MeOH). The dark red band was collected and concentrated to yield red crystals. Yield, 64.8 mg (23.4%). Anal. Calcd for $C_{36}H_{35}KN_2O_{14}Ru_2$ ($K[Ru_2(dhpta)(\mu\text{-}O_2CCH_2\text{-}2\text{-}naph)_2]\cdot CH_3OH$): C, 45.00; H, 3.67; N, 2.92. Found: C, 44.56; H, 3.38; N, 3.05. ESI-MS: *m*/*z* 891.0 $[M - K]^-$ (calcd for $C_{35}H_{31}N_2O_{13}Ru_2$, 891.0). UV−vis ($c$ = 0.256 mM, DMSO, light path length = 1 cm): λ, nm (ϵ, $M^{-1}\,cm^{-1}$) 261 (1.92×10^4), 272 (2.01×10^4), 278 (2.01×10^4), 381 (2.56×10^3), 491 (2.92×10^3). ^{1}H NMR in DMSO-d_6 (300.07 MHz): δ 58.4 (Br, 1H, 2-dhpta*H*), 8.21 (s, 1H, H1-naphthyl), 7.95 (d, 2H, ^3J = 8.8 Hz, H4-naphthyl), 7.79−7.71 (m, 2H, H9, H6-naphthyl), 7.70 (d, 1H, ^3J = 8.8 Hz, H3-naphthyl) 7.58−7.53 (m, 1H, H8-naphthyl), 7.45−7.39 (m, 3H, H7, H6′, H9′-naphthyl), 7.41−7.28 (m, 2H, H7′, H8′-naphthyl), 7.09 (d, 1H, ^3J = 8.8 Hz, H4′-naphthyl), 5.35 (s, 2H, $-CH_2$-naphthyl), 5.21 (s, 1H, H1′-naphthyl), 4.62 (d, 1H, ^3J = 8.8 Hz, H3′-naphthyl), 4.41 (br, 2H, 1,3-dhpta*H*), −1.06 (d, 2H, ^2J = 17.7 Hz, $-N-CH_2-CO_2$), −2.03 (s, 2H, $-CH_2'$-naphthyl), −2.89 (d, 2H, ^2J = 18.3 Hz, $-N-CH_2'$-CO_2), −6.10 (d, 2H, ^2J = 10.8 Hz, 1,3-dhpta*H*′), −6.42 (d, 2H, ^2J = 15.0 Hz, $N-CH_2'$-CO_2), −6.73 (d, 2H, ^2J = 15.3 Hz, $N-CH_2'$-CO_2). IR (KBr, cm^{-1}): 3244, 2361, 1670, 1566, 1508, 1369, 1346, 1286.

Physical Measurements. Electrospray ionization mass spectra (ESI-MS) were recorded on a JEOL JMS-T100LC. Elemental analyses were carried out using a Perkin-Elmer PE2400 Series II CHNS/O Analyzer (Nara Institute of Science and Technology). IR spectra were recorded on a JASCO FT/IR 8900μ as KBr disks. UV−visible (UV−vis) spectra were recorded on a JASCO V-570

(37) Osuka, A.; Nakajima, S.; Maruyama, K.; Mataga, N.; Asahi, T.; Yamazaki, I.; Nishimura, Y.; Ohno, T.; Nozaki, K. *J. Am. Chem. Soc.* **1993**, *115*, 4577.
(38) Nakashima, S.; Taniguchi, S.; Okada, T.; Osuka, A.; Mizutani, T.; Kitagawa, T. *J. Phys. Chem. A.* **1999**, *103*, 9184.
(39) Ozeki, H.; Nomoto, A.; Ogawa, K.; Kobuke, Y.; Murakami, M.; Hosoda, K.; Ohtani, M.; Nakashima, S.; Miyasaka, H.; Okada, T. *Chem.—Eur. J.* **2004**, *10*, 6393.
(40) Obata, M.; Tanihara, N.; Nakai, M.; Harada, M.; Akimoto, S.; Yamazaki, I.; Ichimura, A.; Kinoshita, I.; Mikuriya, M.; Hoshino, M.; Yano, S. *Dalton Trans.* **2004**, *20*, 3283.
(41) Föster, T.; Kasper, K. Z. *Phys. Chem. NF* **1954**, *1*, 275.
(42) Briks, J. B. *Photophysics of Aromatic Molecules*; Wiley-Interscience: London, 1970.
(43) Gravett, D. M.; Guillet, J. E. *Macromolecules* **1995**, *28*, 274.
(44) Roy, B. M.; Samanta, S.; Chattopadhyay, G.; Ghosh, S. *J. Lumin.* **2004**, *106*, 141.
(45) Beeby, A.; Parker, D.; Williams, J. A. G. *J. Chem. Soc., Perkin Trans.* **1996**, 1565.
(46) Karnavos, G. J.; Turro, N. J. *Chem. Rev.* **1986**, *86*, 401.
(47) Juliard, M.; Chanon, M. *Chem. Rev.* **1983**, *83*, 425.
(48) Picraux, L. B.; Weldon, B. T.; McCusker, J. K. *Inorg. Chem.* **2003**, *42*, 273.
(49) Evans, I. P.; Spencer, A.; Wilkinson, G. *J. Chem. Soc., Dalton Trans.* **1973**, 204.

Table 1. Crystallographic and Experimental Data for **2**

formula	$C_{36}H_{35}KN_2O_{14}Ru_2$
fw	960.92
cryst syst	orthorhombic
space group	*Pbca* (No. 61)
unit cell	
a (Å)	10.6200 (5)
b (Å)	20.270 (1)
c (Å)	35.530 (2)
V (Å^3)	7648.5 (7)
Z	8
T (°C)	−80.0
D_{calcd} (g·cm^{-3})	1.669
μ(Mo Kα) (cm^{-1})	9.69
trans factor	0.861−0.986
no. of unique data	8689 ($I > 2\sigma(I)$)
no. obsd data	59400
no. variables	501
R^a	0.052
$R_w{}^a$	0.122
GOF	1.13

^{a} $R = \sum||F_o| - |F_c||/\sum|F_o|$; $R_w = [\sum w(|F_o| - |F_c|)^2/\sum w|F_o|^2]^{1/2}$; $w = 1/\sigma^2(F_o)$.

UV/VIS/NIR spectrometer at room temperature. Static fluorescence spectra were measured at 77 K (liquid nitrogen) in a 1 cm quartz cell with a fluorescence spectrophotometer (Hitachi, F-4500) in EtOH/MeOH = 4/1 (v/v) and corrected for the spectral response of the instrument.^{1}H NMR (300.07 MHz) spectra were recorded on a Varian GEMINI 2000 spectrometer. Cyclic voltammograms were recorded on a BAS CV-50W voltammetric analyzer by using a conventional three-electrode system, a glassy carbon and platinum wire working electrode, a platinum wire counter electrode, and an $Ag/AgPF_6$ (in *N*,*N*-dimethylformamide, DMF, and CH_3CN) reference electrode. All spectra were scanned at 100 mV s^{-1}. Since the $Ag/AgPF_6$ reference electrode had a potential of −0.04 V (in CH_3CN) or −0.09 V (in DMF) versus the ferrocenium/ferrocene ($Fc^{+/0}$) couple as an external standard, potentials reported here were corrected to those versus $Fc^{+/0}$ by adding either −0.04V or −0.09 V to the potential values estimated versus the $Ag^{+/0}$ electrode. Controlled potential electrolysis was carried out with a Nichiakesoku NP-IR 1000 potentiostat. Magnetic susceptibility (μ_{eff}) at room temperature was obtained by the Gouy method. The diamagnetic corrections were calculated from a table of Pascal's constants. The temperature dependence of the magnetic susceptibility was measured on a Quantum Design MPMS-5S SQUID susceptometer operating at a magnetic field of 0.5 T at 4.5−300 K. All data were fitted to the Bleaney−Bowers equation, taking into account the small amount of mononuclear Ru^{III} impurity and temperature-independent paramagnetism ($N\alpha$) as shown in eq 1

$$\chi_M = \frac{2Ng^2{\mu_B}^2}{3kT}\left\{1 + \frac{1}{3}\exp\left(-\frac{2J}{kT}\right)\right\}^{-1}(1-p) + \frac{Ng^2{\mu_B}^2}{2kT}p + 2N\alpha \quad (1)$$

where N, μ_B, k, and p are Avogadro's number, the Bohr magnetron, Boltzmann's constant, and the extent of mononuclear Ru^{III} impurity, respectively.

X-ray Crystallography. Experimental data are summarized in Table 1. A dark red crystal of **2** was mounted on a glass fiber and cooled in a stream of cold nitrogen gas. All data sets were collected on a Rigaku Mercury instrument by using graphite-monochromated Mo Kα radiation with a maximum 2θ value of 55.0°. All data sets were corrected for Lorentz polarization effects and for absorption. The structure of **2** was solved by Patterson methods (DIRDIR-94[50]) and expanded by using Fourier techniques. Hydrogen atoms were added but not refined. The structure of **2** was refined with the full-matrix least-squares technique[51] minimizing $\sum w(|F_o| - |F_c|)^2$, where $w = 1/(\sigma^2(F_o))$. The final refinement with anisotropic thermal parameters for all non-hydrogen atoms was converged with $R = 0.052$ and $R_w = 0.122$. The largest peak in the final differential Fourier map was 0.96 e Å^{-3}.

EXAFS Analysis. Extended X-ray absorption fine structure (EXAFS) measurements were performed at beam line 10B of the Photon Factory of the High Energy Acceleration Research Organization (KEK-PF), Tsukuba, Japan. Measurements of spectra of the DMSO solutions (0.5 mL) of **1** (45 mg) and **2** (50 mg) in bags and analyses of the spectral data were performed in the same manner as reported previously.[36] Spectral analyses were performed by using REX2000, version 2.0.7 (Rigaku Co.).

Preparation of $[Ru^{III}Ru^{II}(dhpta)(\mu\text{-}O_2CCH_2\text{-}R)_2]^{2-}$ (R = 1-naph (6) and R = 2-naph (7)) by the Controlled Potential Electrolysis of 1 and 2. Complexes **1** and **2** and degassed DMF were placed in a cell with a carbon working electrode, a platinum wire counter electrode, and an $Ag/AgPF_6$ reference electrode. Electrolysis was carried out at −1.50 V versus $Ag/AgPF_6$ under Ar until the current flow ceased. The formation of **6** and **7** was confirmed by their characteristic bands in electronic spectra.

Fluorescence Decay Measurement. Fluorescence decay was measured by the time-correlated single-photon-counting method. The excitation light source was third harmonic pulses (295 nm) generated from a mode-locked Ti:sapphire laser (Spectra Physics, Tsunami 3950) that was pumped by an Ar^+ laser (Spectra Physics, BeamLok 2060). The fluorescence emission was detected with a photomultiplier tube (PMT; Hamamatsu Photonics, R3234) through a monochromator (Ritus MC-10N) with two cutoff filters (UV-31) for the excitation light. The details of this apparatus have been described in the literature.[52] The total instrument response function has an fwhm (full width at half-maximum) of ca. 750 ps at the excitation wavelength. The decay data were fitted with the sums of exponential functions that were convoluted with the instrument response function by the nonlinear least-squares method.

Results and Discussion

Preparation and Structures of Complexes 1 and 2. $K[Ru_2(dhpta)(\mu\text{-}O_2CCH_2\text{-}1\text{-}naph)_2]$ (**1**) was synthesized by the direct method,[34] and $K[Ru_2(dhpta)(\mu\text{-}O_2CCH_2\text{-}2\text{-}naph)_2]$ (**2**) was synthesized by a substitution reaction[35] as shown in Scheme 1. For the synthesis of **1**, the reaction of $RuCl_2(DMSO)_4$ in aqueous solution is preferable to that in MeOH since the latter makes it hard to purify the complex by column chromatography. On the other hands, the synthesis of **2** by the ligand substitution reaction gave a higher yield compared with that of the direct method by using $RuCl_2(DMSO)_4$ in aqueous solution. Complexes **1** and **2** were found to be soluble in methanol, ethanol, CH_3CN, DMF, and DMSO. ESI MS spectra of **1** and **2** gave $[M - K]^-$ peaks at 891.2 and 891.0, respectively, consistent with the proposed structures.

The structure of **2** was determined by X-ray crystallography. The unit cell involved the complex anion

(50) Beurskens, P. T.; Admiraal, G.; Beurskens, G.; Bosman, W. P.; de Gelder, R.; Israel, R.; Smits, J. M. M. *The DIRDIR-94 Program System*; Technical Report of the Crystallography Laboratory; University of Nijimegen: Nijimegen, The Netherlands, 1994.
(51) Sheldrick, G. M. *Program for the Refinement of Crystal Structures*; University of Göttingen: Göttingen, Germany, 1997.
(52) Ohkita, H.; Ito, S.; Masahide, Y.; Yasuo, T.; Tani, K. *J. Phys. Chem. A.* **2002**, *106*, 2140.

Scheme 1. Synthetic Procedures of **1** and **2**[a]

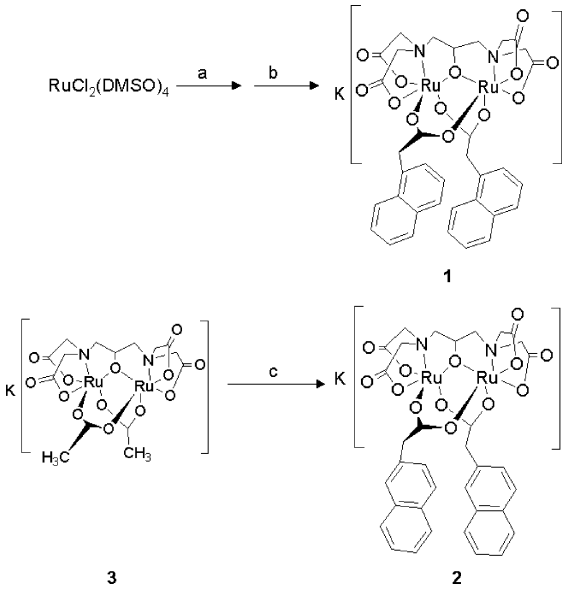

[a] Conditions: (a) addition of H_5dhpta, adjust pH at 5 with 1 M KOH; (b) addition of 1-naphthylacetic acid, keep at 80−85 °C for 3 days; (c) addition of 2-naphthylacetic acid, reflux for 3 days.

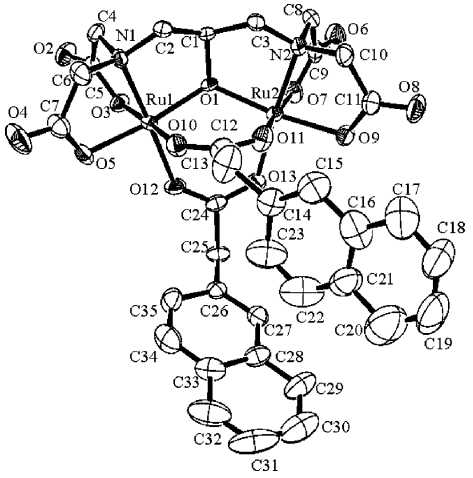

Figure 1. ORTEP drawing of **2** showing 50% probability ellipsoids. The hydrogen atoms, K^+ countercation, and one MeOH molecule have been omitted for clarity.

Table 2. Selected Bond Lengths (Å) and Angles (deg) for **2** with Estimated Standard Deviations in Parentheses

Ru(1)−Ru(2)	3.438(6)	Ru(1)−O(1)	1.956(3)
Ru(1)−O(3)	1.989(3)	Ru(1)−O(5)	2.041(3)
Ru(1)−O(10)	2.052(3)	Ru(1)−O(12)	2.093(3)
Ru(1)−N(1)	2.026(3)	Ru(2)−O(1)	1.962(3)
Ru(2)−O(7)	1.955(3)	Ru(2)−O(9)	2.026(3)
Ru(2)−O(11)	2.051(3)	Ru(2)−O(13)	2.092(3)
Ru(2)−N(2)	2.032(4)		

Ru(1)−O(1)−Ru(2)	122.7(1)	O(1)−Ru(1)−O(10)	87.6(1)
O(1)−Ru(1)−O(12)	97.0(1)	O(10)−Ru(1)−O(12)	90.3(1)
O(1)−Ru(2)−O(11)	87.8(1)	O(1)−Ru(2)−O(13)	99.1(1)
O(11)−Ru(2)−O(13)	89.2(1)		

$[Ru_2(dhpta)(\mu\text{-}O_2CCH_2\text{-}2\text{-}naph)_2]^-$, one potassium cation, and one MeOH molecule. The ORTEP plot of $[Ru_2(dhpta)(\mu\text{-}O_2CCH_2\text{-}2\text{-}naph)_2]^-$ is shown in Figure 1, and selected bond lengths and angles are listed in Table 2. The structure of the complex anion of **2** is similar to that of **3**,[34] with two ruthenium atoms symmetrically bridged by the alkoxide of dhpta and two coordinated naphthyl acetate ligands to give a cofacial bioctahedral structure. The distances of Ru−O and Ru−N are 1.955(3)−2.093(3) Å, and the distance of Ru(1)···Ru(2) is 3.438(6) Å. The angle of Ru(1)−O(1)−Ru(2) is 122.7(1)°. These bond distances and angle are similar to those of **3**. The bond angles of O(10)−Ru(1)−O(12) and O(11)−Ru(2)−O(13) are 90.3 and 89.2°, which are lager than those of **3**. The planes of the naphthyl moieties (deviation from planarity 0.0702 and 0.0661 Å) are nearly perpendicular to each other (74.3°). This angle is similar to that of $[Fe_2(O)(\mu\text{-}O_2CCH_2\text{-}2\text{-}naph)_2(TACN\text{-}Me_3)_2]^{2+}$ (72.4°).[48]

Table 3. Structural Parameters Derived from EXAFS Analysis for Complexes **1**−**3**

	EXAFS					X-ray crystallography	
complex	shell	r[a] (Å)	N[b]	σ	R (%)	r (Å)	N
1	Ru−O/N	2.05	5.3	0.047	2.1		
(solid)	Ru−C	2.89	6.8	0.080			
	Ru−Ru	3.46	0.6	0			
2	Ru−O/N	2.05	5.5	0.044	3.3	2.023	
(solid)	Ru−C	2.86	6.8	0.091		2.833	
	Ru−Ru	3.46	0.4	0		3.438	1.0
1	Ru−O/N	2.05	5.7	0.051	3.7		
(DMSO)	Ru−C	2.83	7.4	0.103			
	Ru−Ru	3.48	0.5	0			
2	Ru−O/N	2.06	5.9	0.056	1.9		
(DMSO)	Ru−C	2.87	7.1	0.085			
	Ru−Ru	3.47	0.4	0			
3	Ru−O/N	2.04[c]	6[c]				
(solid)	Ru−C	2.84[c]	6[c]				
	Ru−Ru	3.44[c]	1[c]			3.433[c]	1.0[c]

[a] Estimated errors are ± 0.01 Å. [b] Estimated errors are ± 0.7. [c] Data from ref 34.

The structures of **1** and **2** in the solid state and in the DMSO solution were studied by EXAFS. In the Fourier transforms of the EXAFS oscillation of **1** and **2** in the solid states and in DMSO (Figure S1), three peaks were found at 1.6, 2.3, 3.0 Å (before phase-shift correction), and these were assigned to the backscattering contribution of the nitrogen and oxygen atoms (N/O) coordinated to ruthenium, the carbon atoms (C) including the five-membered chelate rings, and the ruthenium atom (Ru), respectively. The Fourier-filtered technique was applied in the curve fitting of each peak with three terms, $\boldsymbol{k}^3\chi(\boldsymbol{k})_{N/O}$, $\boldsymbol{k}^3\chi(\boldsymbol{k})_C$, and $\boldsymbol{k}^3\chi(\boldsymbol{k})_{Ru}$, under the assumption of $\boldsymbol{k}^3\chi(\boldsymbol{k}) = \boldsymbol{k}^3\chi(\boldsymbol{k})_{N/O} + \boldsymbol{k}^3\chi(\boldsymbol{k})_C + \boldsymbol{k}^3\chi(\boldsymbol{k})_{Ru}$. Resulting $\boldsymbol{k}^3\chi(\boldsymbol{k})_{calcd}$ and $\boldsymbol{k}^3\chi(\boldsymbol{k})_{obsd}$ values are shown in Figure S1, and the structural parameters (i.e., diatomic distance r, coordination number N, and the Debye−Waller factor, σ) are listed in Table 3. The r values for **1** and **2** in the solid state and in the DMSO solution are similar to those of **3**.[34,36] These results indicated that **1** and **2** have a hemerythrin-like coordination frame similar to that of **3** even in the DMSO solution. The ^{1}H NMR data of **1** and **2** also suggest that the dinuclear structures maintain in DMSO. The ^{1}H NMR spectra of **1** and **2** showed sharp signals in the range of −7∼62 ppm. The peaks at 61.9 and 58.4 ppm are assigned to methine protons because the signals of the methine protons of $K[Ru_2(dhpta)(\mu\text{-}O_2C\text{-}R)_2]$ (R = CH_3 (**3**), C_6H_5 (**4**), and ZnTPP (**5**)) are known to appear at 50.9∼56.9 ppm.[34,36] Three methylene and naphthyl moieties exhibited two sets of peaks because of the C_s symmetry of **1** and **2**. Noticeably, the signals of the acetate functions of the naphthyl moieties were split into

Table 4. Physical Properties of **1** and **2**

	magnetic properties[a]				formal redox potential[b] (V vs $Fc^{+/0}$)				intervalence charge-transfer band[c] (band I)			
					process							
complex	g	$-J$ (cm^{-1})	p	$N\alpha$ ($\times 10^6$ emu mol^{-1})	(i)	(ii)	(iii)	(iv)	ν_{max} ($\times 10^3$ cm^{-1})	$\Delta\nu_{1/2}$ ($\times 10^3$ cm^{-1})	ϵ_{max} ($\times 10^3$ M^{-1} cm^{-1})	H_{ad} ($\times 10^3$ cm^{-1})
1	2.1	581	0.003	435	1.29	0.63 (0.53)	−1.05 (−1.27)	−1.36 (−1.73)	5.8	3.7	0.70	0.73
2	2.1	378	0.026	176	1.30	0.64 (0.54)	−1.05 (−1.28)	−1.34 (−1.71)	5.8	3.7	0.69	0.72

[a] Magnetic parameters derived from the fitting to temperature-dependent molar susceptibility. Determined in the solid. [b] 0.1 M [n-Bu_4N]PF_6; glassy carbon working electrode; $Ag/AgPF_6$ reference electrode. Determined in CH_3CN (and in DMF). Potentials were corrected to those vs $Fc^{+/0}$ by adding either −0.04 V (in CH_3CN) or −0.09 V (in DMF) to the potential values estimated vs the $Ag^{+/0}$ electrode. [c] Determined in DMF.

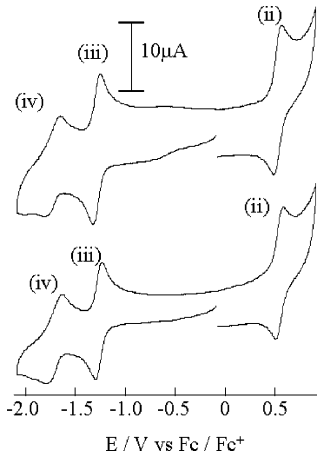

Figure 2. Cyclic voltammograms of (a) **1** and (b) **2** in DMF at scan rate of 100 mV s^{-1}.

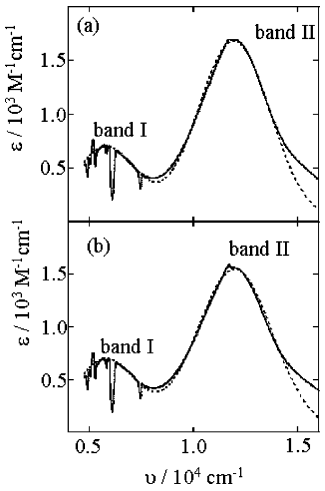

Figure 3. Electronic absorption spectra of (a) **6** and (b) **7** in DMF and fitting data as the intervalence charge-transfer bands (band I and band II) of **6** and **7** (observed spectra (—) and fitting data (- -)).

two signals (i.e., at −1.69 and 5.49 ppm with **1** and at −2.03 and 5.35 ppm with **2**) indicating that the two naphthyl moieties are located in magnetically distinct environments.

Magnetic Properties. Complexes **1** and **2** are paramagnetic at room temperature with a magnetic moment (μ_{eff}) of 1.20 and 1.19 μ_B per Ru^{III} ion. These values are significantly lower than that expected for a low spin d^5 complex (1.73 μ_B), indicating a strong antiferromagnetic interaction between the two Ru^{III} ions. The temperature dependence of the molar magnetic susceptibility (χ_M) of **1** and **2** in the temperature range of 4.5−300 K (Figure S2) was fitted to the Bleaney−Bowers equation,[53] by taking into account of the small amount of a mononuclear Ru^{III} complex present as an impurity and temperature-independent paramagnetism ($N\alpha$) based on the Heisenberg model, $H = -2JS_1S_2$. The g value was fixed to 2.1, and the diruthenium system was treated as a ground-state singlet with a low-lying triplet state. The magnetic parameters of **1** and **2** are listed in Table 4. The large antiferromagnetic coupling constant values ($-J$) of **1** and **2** indicate a significant interaction between unpaired electrons of the two Ru^{III} ions through the μ-alkoxo and μ-carboxylato bridges. The significant sharp ^1H NMR signals of **1** and **2** also suggested the participation of a strong antiferromagnetic interaction between the two Ru atoms.

Electrochemical Properties. As shown in Figure 2, the cyclic voltammograms of **1** and **2** recorded in DMF showed one reversible oxidation peak and two reversible reduction peaks, and all of these peaks corresponded to ruthenium moieties ($E_{1/2}^{(ii)}$) at 0.53 (**1**) and 0.54 V (**2**) and were assigned to the oxidation of $Ru^{III}Ru^{III}$ to $Ru^{IV}Ru^{III}$. The one-electron reduction peaks ($E_{1/2}^{(iii)}$ and $E_{1/2}^{(iv)}$) at −1.27 (**1**) and −1.28 V (**2**) and at −1.73 (**1**) and −1.71 V (**2**) were assigned to the reductions of $Ru^{III}Ru^{III}$ to $Ru^{II}Ru^{III}$ and of $Ru^{II}Ru^{III}$ to $Ru^{II}Ru^{II}$, respectively. The peaks assigned to the naphthalene moieties were not observed in the potential range studied. When the cyclic voltammograms of **1** and **2** were recorded in CH_3CN, the irreversible peaks were observed at 1.29 (**1**) and 1.30 V (**2**), and they were assigned to the oxidation of naphthyl moieties. The large potential differences between $E_{1/2}^{(iii)}$ and $E_{1/2}^{(iv)}$ suggest that **1** and **2** are in the stable mixed-valent state. The conproportionation constants (K_c) of **1** and **2** calculated according to eq 2 were 1.87×10^7 and 8.60×10^6, respectively, indicating the significant stability of the mixed-valent species $[Ru^{II}Ru^{III}(dhtpa)(\mu\text{-}O_2CCH_2\text{-}1\text{-}naph)_2]^{2-}$ (**6**) and $[Ru^{II}Ru^{III}(dhtpa)(\mu\text{-}O_2CCH_2\text{-}2\text{-}naph)_2]^{2-}$ (**7**).

$$[Ru^{III}{}_2L_2]^- + [Ru^{II}{}_2L_2]^{3-} \overset{K_c}{\rightleftharpoons} 2[Ru^{II}Ru^{III}L_2]^{2-}$$

$$K_c = \exp\left\{\frac{F(E_{1/2}{}^{(iii)} - E_{1/2}{}^{(iv)})}{RT}\right\} \qquad (2)$$

The mixed-valent species, **6** and **7**, were prepared by the controlled potential electrolysis of **1** and **2**, respectively, at −1.50 V vs $Ag/AgPF_6$ in DMF. Figure 3 shows the electronic

(53) Bleaney, B.; Bowers, K. *Proc. R. Soc. London, Ser. A* **1952**, *214*, 451.

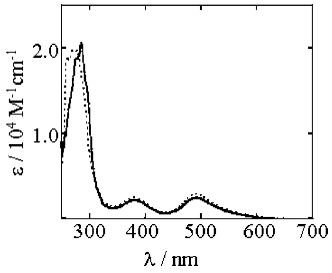

Figure 4. Electronic absorption spectra of **1** (—) and **2** (- -) in DMSO.

absorption spectra of **6** and **7** in the near-IR regions, in which each concentration was determined on the basis of the Ru^{III}_2 complexes restored. These two bands (band I and II) may be assigned to intervalence charge-transfer bands because these two bands are absent in the electronic spectra of **1** and **2**. At the moment, the analysis of band II is not sufficient because alternative assignment to LMCT bands is not thoroughly ruled out. The lower-energy IT band (band I) was analyzed by Gaussian curve fitting to determine the energy of the band maximum, ν_{max}, the maximum extinction coefficient, ϵ_{max}, and the half-height width, $\Delta\nu_{1/2}$ (Table 4). The electron exchange integral, H_{ad}, which is a good index for the magnitude of interaction between the metal centers, was estimated to be 640−870 cm^{-1} by calculation according to the Hush's theory (eq 3).[54,55]

$$H_{ad} = 2.05 \times 10^{-2}\left(\frac{\epsilon_{max}\,\Delta\nu_{1/2}}{\nu_{max}}\right)^{1/2}\left(\frac{\nu_{max}}{r}\right) \qquad (3)$$

The Ru−Ru interatomic distances (r) used in the calculation were derived from EXAFS analyses. The values of H_{ad} indicate weak metal−metal interactions and are comparable to those of **3** and **4** which were reported as Class II-type[56] mixed-valent diruthenium complexes.

Photochemical Properties. The electronic absorption spectra of **1** and **2** were measured in DMSO, EtOH/MeOH (4/1, v/v), and CH_3CN at room temperature (Figure 4 and Table S1). In the DMSO solution, two peaks were observed at 381 and 491 nm with ϵ values similar to those of **3** and **4**. The peaks at 381 and 491 nm are assigned to LMCT from the bridge ligands to Ru atoms.[57] The peaks at 250−350 nm are assigned to the $\pi-\pi^*$ transition in the naphthalene moieties.[48]

Static emission spectra of 1-naphthylacetic acid, 2-naphthylacetic acid, **1**, and **2** were observed at 77 K in EtOH/MeOH = 4/1 (v/v) with exciting at 295 nm. These compounds exhibited both fluorescence (300−400 nm)[44,48] and phosphorescence (400−550 nm).[58] Figure 5 shows the fluorescence spectra after subtracting phosphorescence spectra. The fluorescence spectra of **1** and **2** were broadened in the low energy portion of the emission envelope and their intensities were significantly lower than those of 1- and

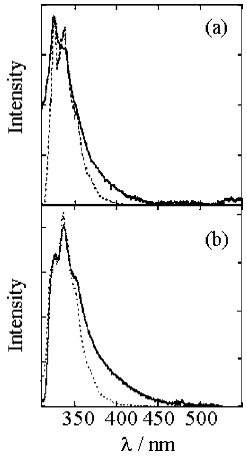

Figure 5. Static fluorescence spectra of (a) 1-naphthylacetic acid (- -) and **1** (—) and (b) 2-naphthylacetic acid (- -) and **2** (—) at 77 K in EtOH/MeOH = 4/1 (v/v). λ_{ex} = 295 nm.

2-naphthylacetic acids. The complex **5** showed also the decrease in the fluorescence intensity but not the broadening. Since the static fluorescence spectrum of $[Fe_2(O)(\mu\text{-}O_2CCH_2\text{-}2\text{-naph})_2(TACN\text{-}Me_3)_2]^{2+}$ was reported to become broadened because of the formation of the excimer,[48] the broadened fluorescence spectra of **1** and **2** suggest the formation of excimer in these complexes. To clarify the reason the spectroscopic feature of the complexes having naphthyl moieties (**1** and **2**) is so different from that of the complex having porphyrin moieties (**5**), the emissions from **1** and **2** were examined in more detail.

The fluorescence lifetimes of **1** and **2** were expected to be very short compared with those of naphthalene because those of **5** were much shorter[40] (36 ps and 540 fs) than those of porphyrin (1 ns and 2 ps).[59] The fluorescence decays of **1** and **2**, together with 1- and 2-naphthylacetic acids for reference, were measured at 77 K in EtOH/MeOH = 4/1 (v/v) because the fluorescence lifetime is known to increase with decreasing temperature. All samples were excited at 295 nm. The monitor wavelength of the fluorescence decays was 340 nm (Figure 6). The fluorescence decays of **1** and **2** were well fitted with the sums of three exponential functions as shown in eq 4 by the nonleast-squares method

$$I(t) = G_1 \exp(-t/\tau_1) + G_2 \exp(-t/\tau_2) + G_3 \exp(-t/\tau_3) \quad (4)$$

where G is the relative amplitude of the fluorescence decay component with lifetime τ.

The fluorescence decay of **1** was fitted by three lifetimes with τ_1 = 78 ns, τ_2 = 2.2 ns, and τ_3 = 1.0 ns. The value, τ_1 = 78 ns, obtained by this deconvolution is very close to the $S_0 \leftarrow S_1$ transition of free 1-naphthylacetic acid (80 ns at 77 K in EtOH/MeOH glassy solid), indicating the presence of 1-naphthylacetic acid as an impurity. The lifetimes, τ_2 and τ_3, are significantly shorter than τ_1 and not characteristic of naphthalene molecules in a glassy solid. These two remarkably short lifetimes suggest the presence of two quenching processes in the fluorescence decay of **1**. These

(54) Creutz, C. *Prog. Inorg. Chem.* **1983**, *30*, 1.
(55) Hush, N. S. *Prog. Inorg. Chem.* **1967**, *8*, 391.
(56) Robin, M. B.; Day, P. *Adv. Chem. Radiochem.* **1976**, *10*, 247.
(57) Sasaki, Y.; Suzuki, M.; Tokiwa, A.; Ebihara, M.; Yamaguchi, T.; Kabuto, C.; Ito, T. *J. Am. Chem. Soc.* **1988**, *110*, 6251.
(58) Kuijt, J.; Ariese, F.; Brinkman, U. A. T.; Gooijer, C. *Anal. Chim. Acta* **2003**, *488*, 135.
(59) Guradyan, G.; Tran-Thi, T.-H.; Gustaavsson, T. *J. Chem. Phys.* **1998**, *108*, 385.

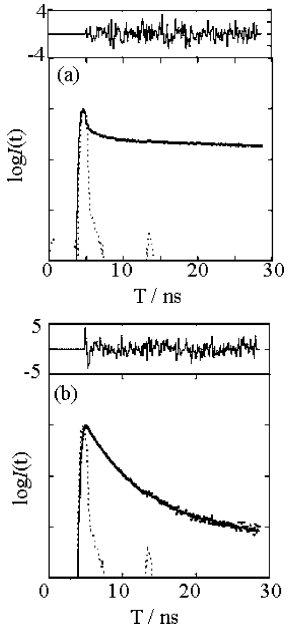

Figure 6. Fluorescence decay of (a) **1** and (b) **2** at 77 K in EtOH/MeOH = 4/1 (v/v): fitting data (—) and pulse data (- -). λ_{ex} = 295 nm; λ_{em} = 340 nm.

Table 5. Fluorescence Decay Parameters of **1** and **2**[a]

complex	monitored wavelength (nm)	τ_1 (ns) (G_1)	τ_2 (ns) (G_2)	τ_3 (ns) (G_3)	χ^2 [b]
1	340	77.9 (0.296)	2.2 (0.401)	1.0 (0.666)	1.12
2	340	14.6 (0.041)	2.3 (0.787)	0.8 (0.570)	1.35
2	400	9.6 (0.018)	1.6 (1.152)	0.7 (0.510)	1.36

[a] The fluorescence decay, $I(t)$, was fitted with sums of three exponential functions as in te equation, $I(t) = G_1 \exp(-t/\tau_1) + G_2 \exp(-t/\tau_2) + G_3 \exp(-t/\tau_3)$, where G is the relative amplitude of the fluorescence decay component with lifetime τ. All samples were measured at 77 K. [b] χ-squared value.

two processes were also observed with **2**, which exhibited three exponential fluorescence decays with lifetimes of τ_1 = 14 ns, τ_2 = 2.3 ns, and τ_3 = 0.8 ns (Table 5). The τ_1 = 14 ns lifetime suggests presence of some unknown impurity other than 2-naphthylacetic acid. Since the excimer formation was suggested from the broadened static fluorescence spectra of **1** and **2**, these short quenching processes with τ_2 and τ_3 may reflect the electron or energy transfer from the excimer and monomer states of naphthalene to Ru centers.

Considering that the $G_2\tau_2/G_3\tau_3$ ratio, which reflects the intensity ratio of the τ_2 and τ_3 components on the static fluorescence spectra,[60,61] is ca. 1.3/1 (**1**) and 4.0/1 (**2**) and that the static fluorescence spectrum of **2** is more broadened than that of **1**, the component for τ_2 (2.0 ± 0.4 ns) can be assigned to the excimer. This is supported by the result that the τ_2 component increases with increasing monitor wavelength. Thus, by varying the monitor wavelength from 340 to 400 nm, the $G_2\tau_2/G_3\tau_3$ ratio of **2** changed from 4.0/1 to 5.2/1. The decrease in the relative value of $G_3\tau_3$, on the other hands, suggests that the τ_3 component corresponds to monomer.

In the photochemical procedure, two types of quenching process (i.e., inter- and intramolecular processes) should be considered. Since the emission lifetimes of **1** and **2** were not affected by the concentration of the complexes at around 10^{-6} M, a bimolecular quenching process can be ignored. Alternatively, intramolecular quenching via energy or electron transfer from the naphthalene to the Ru centers accounts for τ_2 and τ_3. As for the τ_2 quenching process from the excimer, the result that the emission and LMCT take place in the same wavelength region suggests the energy transfer quenching process from the excimer state of naphthalene moieties to the Ru centers. The LMCT bands of **1** and **2** are observed at 381 nm, but the peak positions of the excimer should be estimated since the static fluorescence spectra of complexes **1** and **2** do not show two split bands. Since the excimer emission of naphthalene is observed at 400−450 nm,[44,62] the excimers of **1** and **2** which are conformationally less stable than naphthalene are presumed to exhibit a band at <400 nm.[63,64] Considering that the peak positions of the excimer is generally greater than those of the monomer and that the peak positions of the monomer of **1** and **2** are 327 and 338 nm, the emissions of the excimer of complexes **1** and **2** are estimated to take place at 340−400 nm, which overlaps with LMCT. This facilitates the efficient Förster energy transfer from the naphthalene to the Ru-alkoxo core, since LMCT likely reabsorbs some of the excimer emission from the naphthyl moieties in **1** and **2**. As for the τ_3 quenching process from the monomer, the electron transfer from the monomer state of naphthalene moiety to the Ru centers seems to be probable because the free energy change for the charge separation, which can be estimated to be −1.66 eV from the CV, UV and the fluorescence spectral data (Figure S3)[7,40] suggest that the S_1 state of naphthalene, but not porphyrin, has enough energy to reduce the ruthenium centers.

On the basis of the fact that the excimer of naphthalene is the most stable in the cofacial conformation,[65,66] the excimer of **2**, in which the angle of the two naphthalene planes is 74°, is presumed to be less stable. Compared with **2**, $[Fe_2(O)(\mu\text{-}O_2CCH_2\text{-}2\text{-}naph)_2(TACN\text{-}Me_3)_2]^{2+}$ in which the angle of the two naphthalene planes is 72.4°, is more stable and shows only excimer emission. Since there are no remarkable difference between **1** and **2** in redox potentials, UV spectra, and fluorescence spectra, the result that the relative excimer component is larger in **2** than it is in **1** suggests an important effect of the structural conformation on the excimer emission process. Considering that the structural difference between **1** and **2** comes from the

(60) Amano, F.; Tanaka, T.; Funabiki, T. *J. Mol. Catal. A* **2004**, *221*, 89.
(61) Kato, Y.; Yoshida, H.; Hattori, T. *Phys. Chem. Chem. Phys.* **2000**, *2*, 4231.
(62) Melo, J. S. D.; Pina, J.; Pina, F.; Lodeiro, C.; Parola, A. J.; Lima, J. C.; Albelda, M. T.; Clares, M. P.; Garcia-Espana, E. *J. Phys. Chem. A* **2003**, *107*, 11307.
(63) Yanagitate, M.; Takayama, K.; Takeuchi, M.; Nishimura, J.; Shizula, H. *J. Phys. Chem.* **1993**, *97*, 8881.
(64) Ohkita, H.; Ito, S.; Yamamoto, Y.; Tohda, Y.; Tani, K. *J. Phys. Chem. A* **2002**, *106*, 2140.
(65) Hirayama, F. *J. Chem. Phys.* **1965**, *42*, 3163.
(66) Terazima, M.; Cai, J.; Lim, E. C. *J. Phys. Chem. A.* **2000**, *104*, 1662.

naphthyl moieties, it is probable that the excimer emission is sensitive to the conformation of the naphthyl moieties, especially to the static interaction of two naphthyl moieties. The importance of the static interaction of the photofunctional groups explains why there is no interaction between the porphyrin moieties in complex **5**, in which the angle of the two porphyrin planes is almost 90°. Considering that the photofunctional groups and the carboxylate group are bound through the CH_2 group in **1** and **2** but not in **5**, it is probable that the CH_2 group plays a role for changing the angle of the naphthyl planes. This suggests that further efficient interactions between not only the naphthalene analogues but also porphyrin derivatives become probable by the CH_2 chain length.

Conclusion

New diruthenium complexes having the naphthyl moieties (i.e., $K[Ru_2(dhpta)(\mu\text{-}O_2CCH_2\text{-}1\text{-}naph)_2]$ (**1**) and $K[Ru_2(dhpta)(\mu\text{-}O_2CCH_2\text{-}2\text{-}naph)_2]$ (**2**)) were synthesized, and their photochemical properties, including excimer formation, were characterized. These complexes keep their dinuclear structures both in the solid state and in DMSO solution. Different from those of the other diruthenium complexes without naphthyl moieties, **3**−**5**, the broadened static fluorescence spectra of **1** and **2** suggest the formation of an excimer. The fluorescence decays of **1** and **2** indicate that there are two quenching processes which result from the excimer and monomer states. The short excimer lifetimes of **1** and **2** are the result of the energy transfer from the naphthyl moieties to the Ru centers. The observation that the ratio of the excimer emission is different between **1** and **2** suggests that the excimer formation depends on the interaction between the two naphthyl moieties and, therefore, on the conformation of naphthyl moieties in the diruthenium complexes. Compared with diiron complexes, the diruthenium complexes having photofunctional naphthyl moieties, and their analogues are advantageous for formation of stable mixed-valent states and are expected to be developed for efficient photofunctional complexes and photocatalysts.

Acknowledgment. This work was supported by Grants-in-Aid for Scientific Research on Priority Areas (417, 434), by Grants 13557211, 15033246, 16350032, 17029040, and 17036041 from the Ministry of Education, Culture, Sport, Science and Technology (MEXT) of the Japanese Government, and by grants from Osaka Gas and San-EiGen Foundation for chemical research. The X-ray absorption spectral study has been performed under the approval of the Photon Factory Program Advisory Committee (Proposal No. 2004G290).

Supporting Information Available: X-ray crystallographic file of **2** in CIF format, Fourier transforms of the EXAFS oscillation of **1** and **2** (Figure S1), temperature dependence of the molar magnetic susceptibilities and effective magnetic moments of **1** and **2** (Figure S2), energy diagrams of (a) **1** and **2** and (b) **5** (Figure S3), and UV and fluorescence spectral data of **1** and **2** (Table S1). This material is available free of charge via the Internet at http://pubs.acs.org.

IC051582U